Novel plant flavonoid electrochemical sensor based on in-situ and controllable double-layered membranes modified electrode

Jing Hu[1], **Renjie Zhou**[1], **Hongwei Lin**[1], **Qiuyuan Wei**[2], **Feilong Hu**[2]*, **Xin Yang**[1,3]*

1 Huaihua Key Laboratory for Preparation of Ceramics Materials and Devices, Hunan Engineering Laboratory for Preparation Technology of Polyvinyl Alcohol Fiber Material, Huaihua University, Huaihua, PR China, **2** Guangxi Key Laboratory of Chemistry and Engineering of Forest Products, Guangxi University for Nationalities, Nanning, PR China, **3** Key Laboratory of Research and Utilization of Ethnomedicinal Plant Resources of Hunan Province, Key Laboratory of Hunan Higher Education for Western Hunan Medicinal Plant and Ethnobotany, Huaihua University, Huaihua, PR China

* hflphd@163.com (FH); 01yangxin@163.com (XY)

Abstract

Identification and quantification of plant flavonoids are critical to pharmacokinetic study and pharmaceutical quality control due to their distinct pharmacological functions. Here we report on a novel plant flavonoid electrochemical sensor for sensitive and selective detection of dihydromyricetin (DMY) based on double- layered membranes consisting of gold nano-particles (Au) anchored on reduced graphene oxide (rGO) and molecularly imprinted poly-mers (MIPs) modified glassy carbon electrode (GCE). Both rGO-Au and MIPs membranes were directly formed on GCE via in-situ electrochemical reduction and polymerization processes step by step. The compositions, morphologies, and electrochemical properties of membranes were investigated with X-ray powder diffractometry (XRD), Fourier transform infrared spectrum (FTIR), Field emission scanning electron microscopy (FESEM) combined with various electrochemical methods. The fabricated electrochemical sensor labeled as GCE│rGO-Au/MIPs exhibited excellent performance in determining of DMY under optimal experimental conditions. A wide linear detection range (LDR) ranges from 2.0×10^{-8} to 1.0×10^{-4} M together with a low limit of detection (LOD) of 1.2×10^{-8} M ($S/N = 3$) were achieved. Moreover, the electrochemical sensor was employed to determine DMY in real samples with satisfactory results.

Introduction

Dihydromyricetin (DMY) is the most bioactive and abundant plant flavonoid found in the leaves of Ampelopsis grossedentata (a traditional herbal tea in Huaihua region of China and its alternative name is vine tea). The health beneficial properties of DMY cover anticancer, anti-microbial, antioxidant, anti-inflammatory, antidiabetic, and neuroprotective effects. There-fore, the identification and quantification of it, and investigation of the biological activities have aroused increasing awareness [1, 2]. At present, identification and quantification of DMY

mainly focus on chromatographic and spectral techniques including high-performance liquid
chromatography (HPLC) [3], high-speed countercurrent chromatograph (H-SCC) [4], LC-
mass spectrometry (MS)/MS (LC-MS/MS) [5], and fluorescence spectroscopy (FS) [6]. Unfor-
tunately, expensive instruments or complicated pretreatments are usually required in these
time-consuming and skills-training techniques.

Compared with chromatographic and spectral techniques mentioned above, electrochemi-
cal techniques (ETs) possess advantages of simplicity, celerity, sensitivity, and inexpensive.
Furthermore, the ETs can help to identify the redox of drug compound and offer significant
information related to pharmacokinetic. Thus, interests in analysis of flavonoids by applying
ETs have been increasing. However, few reports are related to voltammetric and electrochem-
istry determination of DMY up to now. For instance, Xu and Zou fabricated the DMY voltam-
metric sensors based on glassy carbon electrode (GCE) modified with SWCNs dispersed in
nafion and DNA immobilizing on En/PGA [7, 8]. The sensitive and simple electrochemical
sensor for determining DMY based on graphene (Gr)-nafion film modified GCE was con-
structed by Wang and his group [9]. Beyond these, there are no other reports.

Currently, more and more researches are being made efforts to provide novel modifiers
toward the electrochemical sensors with better sensitivity and selectivity. Extensive studies
indicated that Gr and its derivative reduced graphene oxide (rGO) are promising and
advanced carbon based nano-materials. Moreover, the stupendous features of large surface
area, high stability, and excellent mobility of charge carriers make them ideal platforms for
anchoring various noble metal particles in the fields of electrochemical sensing. In particular,
rGO supported gold nanoparticles (Au) provide amplified electrical conductivity performance
owe to the acceleration of charge transfer from substrates to nanoparticles. The hybridization
between the sp^2 dangling bonds of rGO resident defect sites and Au is beneficial to improve
stability of nanocomposite [10–12]. Many researches make the combination of them as elec-
trode modifiers for detection of hydrogen peroxide, dopamine, NADH, methylparaben, and
aflatoxin B1 [10–14], etc. Due to good recognition and enrichment abilities to target molecules
together with many other advantages including stability, inexpensive, simplicity, and reusabil-
ity compare with natural biological receptors, molecularly imprinted polymers (MIPs) have
been regarded as ideal artificial recognition elements to improve the measuring selectivity for
electrochemical sensor in complicated matrices [15–17]. Numerous MIPs modified electrodes
were fabricated and used widely in determination of quercetin, amyloid-β protein, chlorpyri-
fos, and azithromycin [18–21], etc. However, drawbacks of slow mass transfer, low binding
capacity, and poor binding kinetics resulted from these organic materials. The challenges are
expected to be solved by incorporating high conductivity nanomaterials. To the best of our
knowledge, there are no reports based on neither rGO-Au nanocomposite nor MIPs modified
electrode to quantitative analysis of DMY till now.

Based on our previous researches in Gr-based nanocomposite and MIPs [10, 11, 18], this
investigation aims at fabricating a novel DMY electrochemical sensor based on double-layered
membranes consisting of rGO-Au nanocomposite and MIPs modified GCE (labeled as
GCE│rGO-Au/MIPs). Both rGO-Au and MIPs membranes were formed on GCE via in-situ
electrochemical reduction and polymerization processes step by step. Compared with previ-
ously published electrochemistry methods for DMY detection, the strategies involved in elec-
trode modifying procedures have following advantages: (i) the electrochemical reduction and
polymerization processes are not only in-situ but also controllable, facile, and rapid, avoiding
complex and time-consuming modification processes. (ii) the usage of precursors such as gra-
phene oxide (GO), gold (III) chloride trihydrate (HAuCl$_4$·3H$_2$O), and acrylamide (AM) is
nearly 100%, reducing the waste of reagents. (iii) no hazardous reducing chemicals or exten-
sive organic solvents was used, and the approach is environmental friendly. Attributing to

reasonable synergistic effects of double-layered membranes, the GCE│rGO-Au/MIPs electrode showed superior sensitivity and selectivity. Meanwhile, the electrochemical sensor was employed to determine DMY in real samples with high accuracy and recovery, which holds great potential application in the future.

Experimental section

Instruments and reagents

The crystallization degrees and phase purity of composites were characterized with Rigaku Ultima IV X-ray powder diffractometer (XRD). The samples with KBr pellets were determined by Shimadzu IR prestige-21 Fourier transform infrared spectroscopy (FTIR). The morphologies characterization of different electrodes were carried on Zeiss Sigma HD Field emission scanning electron microscopy (FESEM) connected to Oxford instruments X-Max^N energy-dispersive X-ray spectrometer (EDS). Under room temperature and N_2 protection, all electrochemical experiments were performed on CH Instruments CHI 660E electrochemical workstation (EW). The EW employed with modified/bare GCE (Φ:3 mm), saturated calomel electrode (SCE), and platinum wire electrode as working, reference, and counter electrodes, respectively. The determination of DMY in Ampelopsis grossedentata samples was also carried out on Shimadzu LC-20AT HPLC.

DMY ($\geq$98%, HPLC) was supplied by Sigma-Aldrich (USA). The stock solution of DMY was stored at 4 ˚C darkly and diluted just before use. The Ampelopsis grossedentata was purchased from Laifeng Jinqi Tengcha Bio Co., Ltd (Enshi, China). The plant materials were identified based on plant morphology by Dr. Zhaotun Hu in the College of Biological and Food Engineering, Huaihua University (Huaihua, China). Graphite powder was obtained from XFNANO Materials Tech Co., Ltd (Nanjing, China). Nafion solution used in membranes formation (0.5 wt.%), $HAuCl_4 \cdot 3H_2O$ with purity of 99.99%, AM, azobisisobutyronitrile (AIBN), ethylene glycol dimethacrylate (EGDMA), and other chemicals were provided by Sinopharm Medicine Holding Co., Ltd (Shanghai, China). Various proportions of NaH_2PO_4 (0.1 M) and Na_2HPO_4 (0.1 M) were mixed to obtain different pH values phosphate buffer (PB) electrolyte solutions.

Fabrication of modified electrodes

The GCE│rGO-Au electrode was fabricated via an in-situ electrochemical reduction with precursors of GO and $HAuCl_4 \cdot 3H_2O$ simultaneously [22]. Firstly, the traditional Hummers method was employed to prepare GO with graphite powder [23, 24]. 0.5 mg of ground GO and 1.0×10^{-5} mol of $HAuCl_4 \cdot 3H_2O$ were dissolved in 1.0 mL of 0.5 wt.% nafion solution to prepare the homogenous dispersion. Then, 6.0 μL of dispersion was cast onto polished GCE and heated by an infrared lamp till dry. Finally, The formation of rGO-Au nanocomposite on GCE was achieved by employing a potential at -1.0 V (vs. SCE) in H_2SO_4 (0.1 M) for 600 s. In control experiments, rGO and Au were formed on GCE by applying same electrochemical reduction approach under similar experimental conditions (labeled as GCE│rGO and GCE│Au).

The DMY-MIPs polymer membrane modified GCE│rGO-Au was fabricated by an in-situ polymerization method [25]. 1.0 mL of porogen solvent (acetonitrile) was added with 0.1 mmol of functional monomer (AM) and 0.025 mmol of template molecule (DMY), and dissolved with ultrasonic. After that, 0.08 mmol of initiator (AIBN) and 1.5 mmol of cross-linking agent (EGDMA) were added. The polymerization solution was deoxygenated by bubbling N_2 for 15 min. 5.0 μL of the mixture was uniformly coated onto GCE│rGO-Au electrode and heated by an infrared lamp till a dry and transparent membrane appeared. Finally, the

modified electrode was immersed into an acetic acid/methanol mixture solution (v/v = 1:1) for 30 min to extract the template molecules of DMY from imprinted membrane and obtained the GCE│rGO-Au/MIPs electrode. Under same conditions in absence of DMY, non-imprinted membrane modified GCE│rGO-Au was prepared (labeled as GCE│rGO-Au/NIPs). All modified electrodes were stored in dry and ambient condition for further electrochemical measurements.

Electrochemical measurements

The electrochemical performances of different electrodes were investigated by electrochemical impedance spectroscopy (EIS, Applied potential: +0.2 V. Frequency range: 0.01–100 K Hz. Amplitude: 5 mV), cyclic voltammetry (CV, Low E: -1.0 V. High E: +1.0 V. Scan rate: 100 mV·s^{-1}. Sample interval: 0.001 V), and differential pulse voltammetry (DPV, Init E: -0.2 V. Final E: +0.6 V. Amplitude: 0.05 V). After each run, the GCE│rGO-Au/MIPs electrodes were eluted with acetic acid/methanol mixture solution for 30 min to make sure no redox currents of the modified electrode were observed, confirming the total removal of DMY from imprinted membrane and obtaining the reusable electrodes. The schematic diagram for fabrication of modified electrode is shown in Fig 1. The real samples of Ampelopsis grossedentata after pretreatments were followed the described procedures as recommended above.

Results and discussions

Characterization of membranes

The XRD spectra of GO, rGO, rGO-Au, and rGO-Au/MIPs are showed in Fig 2. After oxidation, characteristic peak at 2θ = 26˚ corresponding to graphite disappeared and was substituted for a distinct peak of GO at 2θ = 10.8˚ (Fig 2a) [26]. The (002) peak at 2θ = 26˚ exhibits the crystalline feature of Gr, indicating the formation of rGO via an electrochemical reduction of GO (Fig 2b) [27]. The diffraction peaks related to rGO (002) and Au (311), (220), (200), (111) can be observed obviously in rGO-Au nanocomposite (Fig 2c) [22]. The results imply the in-situ electrochemical reduction strategy is efficient for simultaneous formation of rGO-Au nanocomposite. No peaks associate with impurities were found in rGO-Au/MIPs composites (Fig 2d).
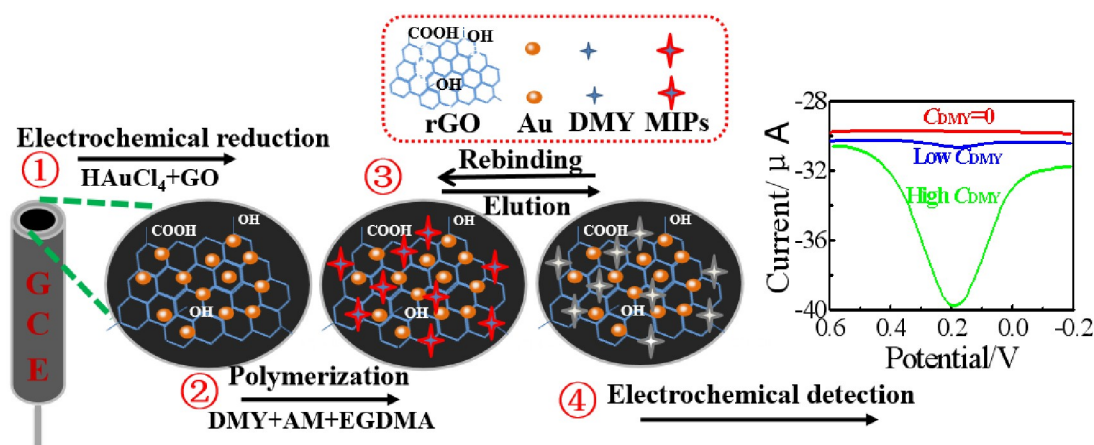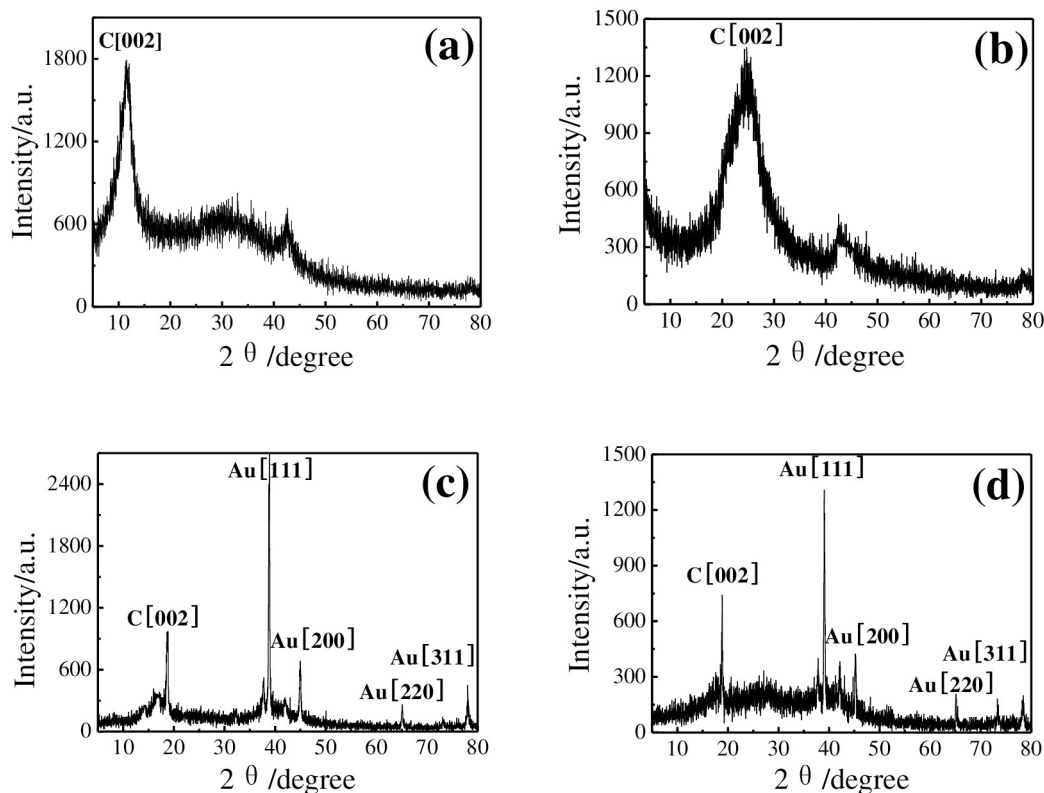

Fig 1. Schematic diagram for fabrication procedures of GCE│rGO-Au/MIPs.
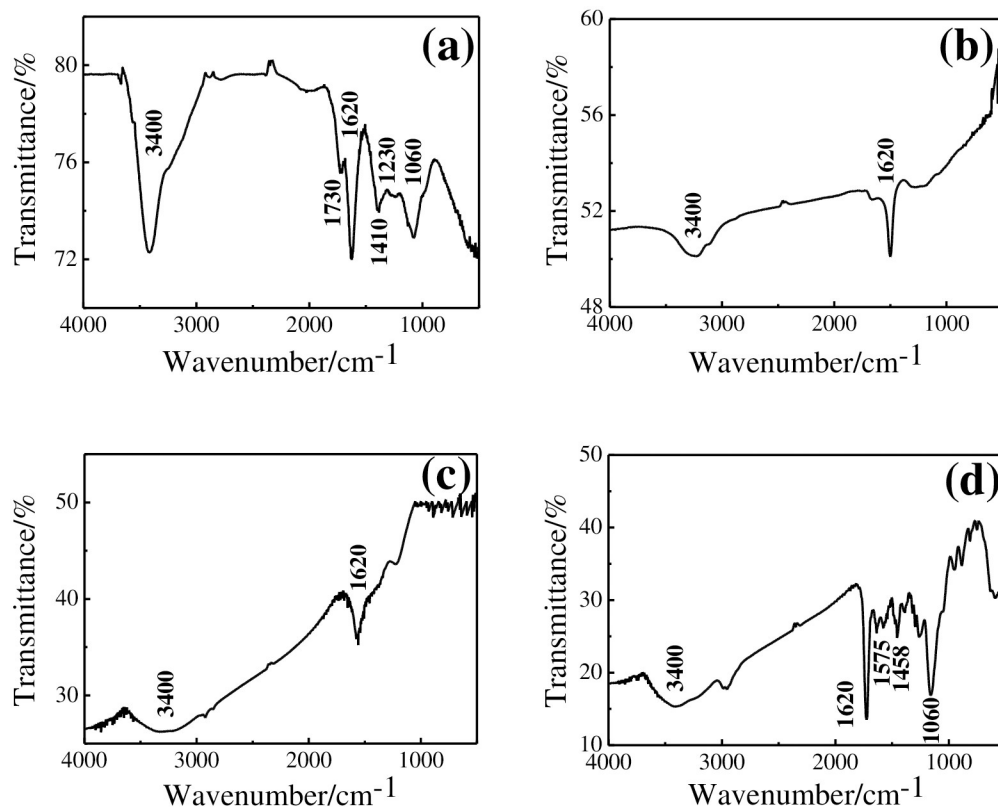
Fig 2. XRD spectra of GO (a), rGO (b), rGO-Au (c), and rGO-Au/MIPs (d).

The FTIR spectrum of GO displays alkoxy (1060 cm^{-1}), aromatic C = C (1620 cm^{-1}), carboxyl C-O (1410 cm^{-1}), C = O (1730 cm^{-1}), epoxy C-O (1230 cm^{-1}), and -OH (3400 cm^{-1}) (Fig 3a) [28]. The remained skeletal vibration at 1620 cm^{-1} related to Gr and disappearance of most oxygen-containing groups in Fig 3b indicate formation of rGO [24]. The absorbance bands of rGO-Au were little changed (Fig 3c). Many adsorption peaks located between 2000 cm^{-1} and 1000 cm^{-1} presence in spectrum of rGO-Au/MIPs (Fig 3d) can be classified to the organic groups introduced by DMY, EDGMA, and AM in MIPs [18].

The continuous and crumpled nanosheets of rGO appeared on GCE (Fig 4a), which are beneficial for maintaining large surface area and anchoring Au. Massive uncapped Au nanoparticles with particle size about 60 nm were uniformly anchored on rGO nanosheets (Fig 4b). The detectable elements shown in EDS spectrum of rGO-Au nanocomposite including C, O, F, and Au (Fig 4f). Most of C originate from rGO. The F and O mainly come from the nafion and functional groups of oxygen- containing in rGO, respectively. The peak at 2.1 keV belongs to Au. Both rGO and Au can amplify electrical conductivity and enlarge specific surface area. The morphologies among GCE│rGO-Au/NIPs (Fig 4c), GCE│rGO-Au/MIPs before (Fig 4d), and after (Fig 4e) template removal are different. The MIPs membrane became rougher after templates removal compared with before templates removal and non-imprinted membrane. The rougher imprinted membrane is good for enhancing rebinding efficiency and improving response selective [25].

Fig 3. FTIR spectra of GO (a), rGO (b), rGO-Au (c), and rGO-Au/MIPs (d).

Characterization of electrochemical performances

The interfacial properties of 0.1 M KCl solution containing 10 mM $K_3[Fe(CN)_6]^{3-/4-}$ as probes on different electrodes were studied with EIS (Fig 5). Randles equivalent circuit model in inset was used to fit EIS results, in which Rct indicates the interfacial electron-transfer impedance of probes on electrode surface and Rct changes with various membranes modified onto GCE. The GCE showed the smallest semicircle diameter and a negligible Rct (10 Ω) (Fig 5a). Due to the nafion in membrane blocks the $[Fe(CN)_6]^{3-/4-}$ diffusion though rGO-Au nanocomposite is electrical conductive, the Rct of GCE│rGO-Au electrode (Fig 5b) increased a little (330 Ω) [24]. The Rct (881 Ω) increased remarkably after modified with MIPs before elution of templates (Fig 5c), showing that the MIPs has been successfully immobilized on the membrane of rGO-Au. The non-conductive MIPs membrane forms barrier between solution and electrode, and blocks exchange of electrons [20]. The Rct (649 Ω) decreased a little after elution of templates (Fig 5d), showing that the templates were removed and the cavities formed. The Rct (812 Ω) located between MIPs before and after elution of DMY when immobilized rGO-Au/ NIPs with similar process (Fig 5e). The phenomenon can be interpreted that the NIPs hinder electron exchange while the absence of DMY can accelerate electron exchange [18]. The results demonstrated that double-layered membranes of rGO-Au and MIPs have been step by step immobilized on GCE.

The electrochemical behaviors of 20.0 μM DMY in pH = 6.0 PB recorded by different electrodes are shown in Fig 6. Generally, the electrochemical reaction of DMY can be appeared as an irreversible anodic peak current (Ipa) on all electrodes. The lowest Ipa for DMY on GCE
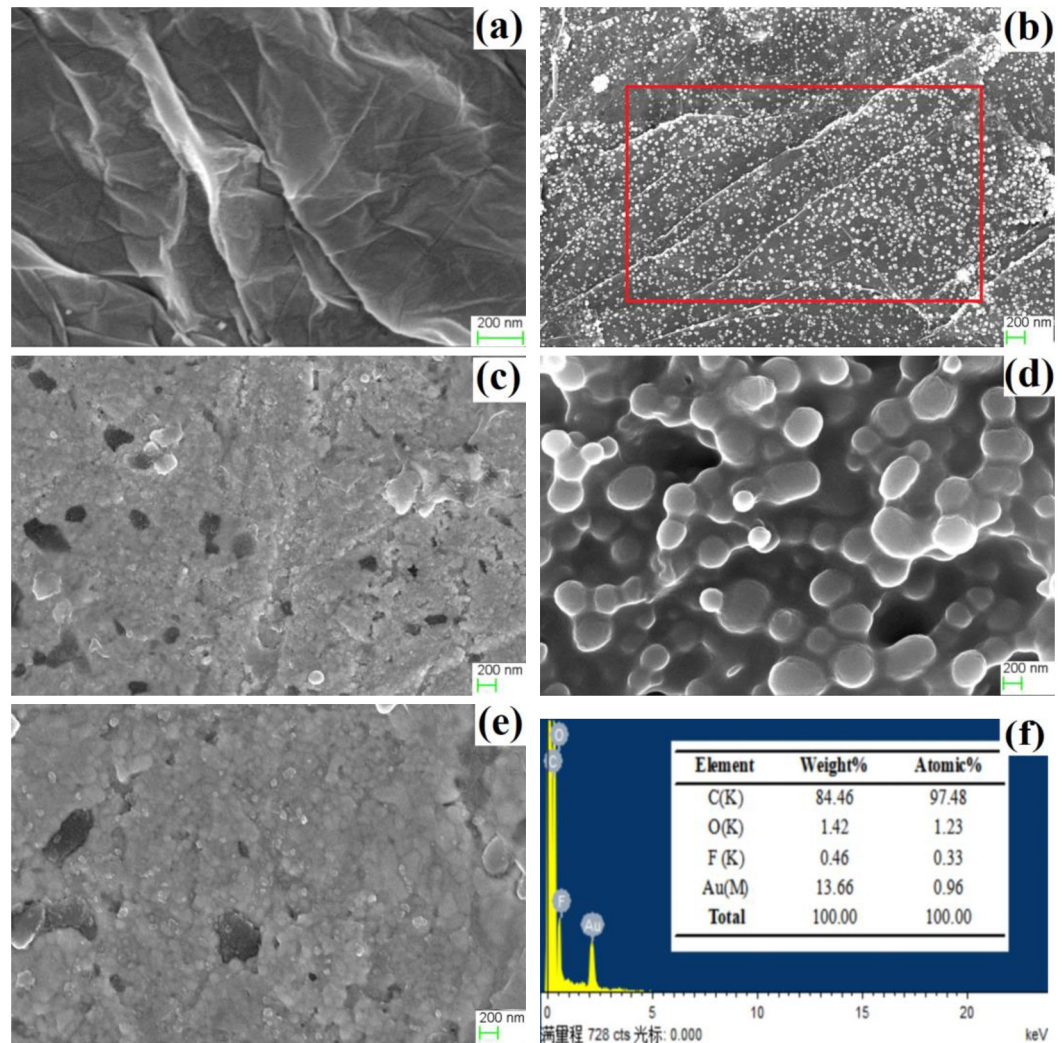
Fig 4. FESEM of GCE│rGO (a), GCE│rGO-Au (b), GCE│rGO-Au/NIPs (c), GCE│rGO-Au/MIPs before (d), after (e) template removal, and EDS of marked area in FESEM image of GCE│rGO-Au (f).

was found at+0.19 V (Fig 6a). Both Ipa and background current increased on GCE│rGO, GCE│Au and GCE│rGO-Au electrodes (Fig 6a', 6a" and 6b). These results can be deduced to the immobilized of rGO, Au, and rGO-Au nanocomposite on GCE are highly conductive, which affords porous structure for electron exchanging of DMY [10]. The Ipa of GCE│rGO-Au/MIPs electrode (Fig 6c) is larger than GCE, GCE│rGO, GCE│Au, and GCE│rGO-Au electrodes, indicating that MIPs has adsorption capacity toward DMY. However, the response of GCE│rGO-Au/NIPs electrode (Fig 6d) is lower than GCE│rGO-Au electrode but still higher than GCE. This can be explained by the synergistic effect of rGO-Au nanocomposite in current amplification exceeds the electron hinder effect of NIPs in current reduction. In addition, the Ipa of GCE│rGO-Au/MIPs electrode increased with higher DMY concentration (Fig 6e). These results confirm the potential application of GCE│rGO-Au/MIPs electrode in DMY analysis.
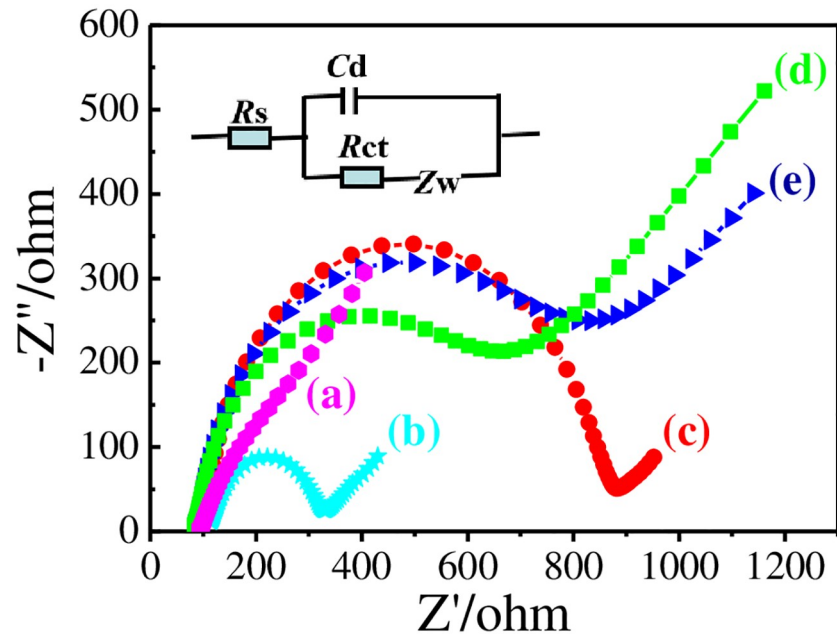
Fig 5. EISs of 0.1 M KCl solution containing 10 mM K$_3$[Fe(CN)$_6$]$^{3-/4-}$ on GCE (a), GCE│rGO-Au (b), GCE│rGO-Au/MIPs before (c), after elution (d), and GCE│rGO-Au/NIPs (e).

Optimization of the experimental parameters

Volume of GO-HAuCl$_4$·3H$_2$O-nafion dispersion. The volume of GO-HAuCl$_4$·3H$_2$O-nafion dispersion on GCE is an important parameter for determining DMY. Several

Fig 6. CVs of 20.0 μM DMY on GCE (a), GCE│rGO (a'), GCE│Au (a"), GCE│rGO-Au (b), GCE│rGO-Au/MIPs (c), GCE│rGO-Au/NIPs (d), and (c) added with 40.0 μM DMY (e).

Fig 7. FESEM of GCE│rGO-Au with electrochemical reduction time of 200 s (a), 400 s (b), 600 s (c), 800 s (d), and their electrochemical performances toward 20.0 μM DMY (e).
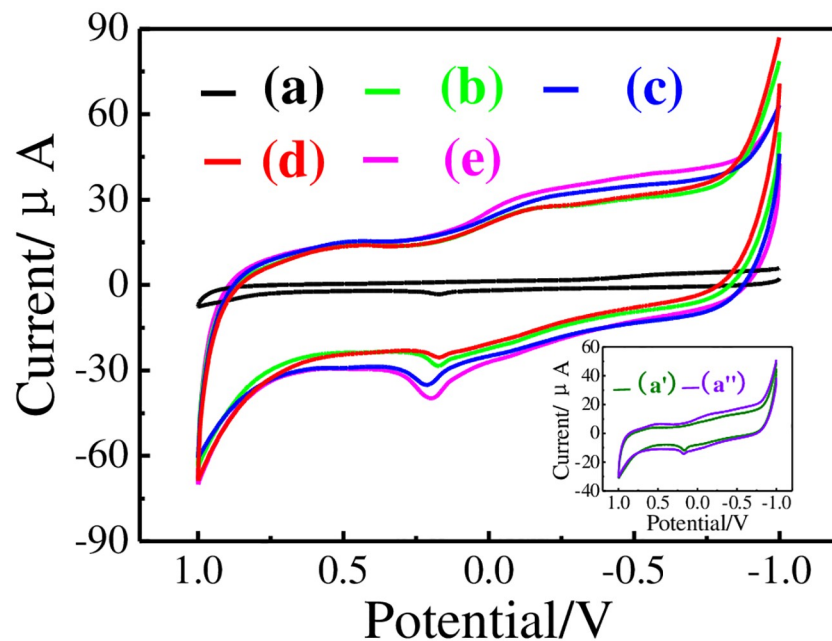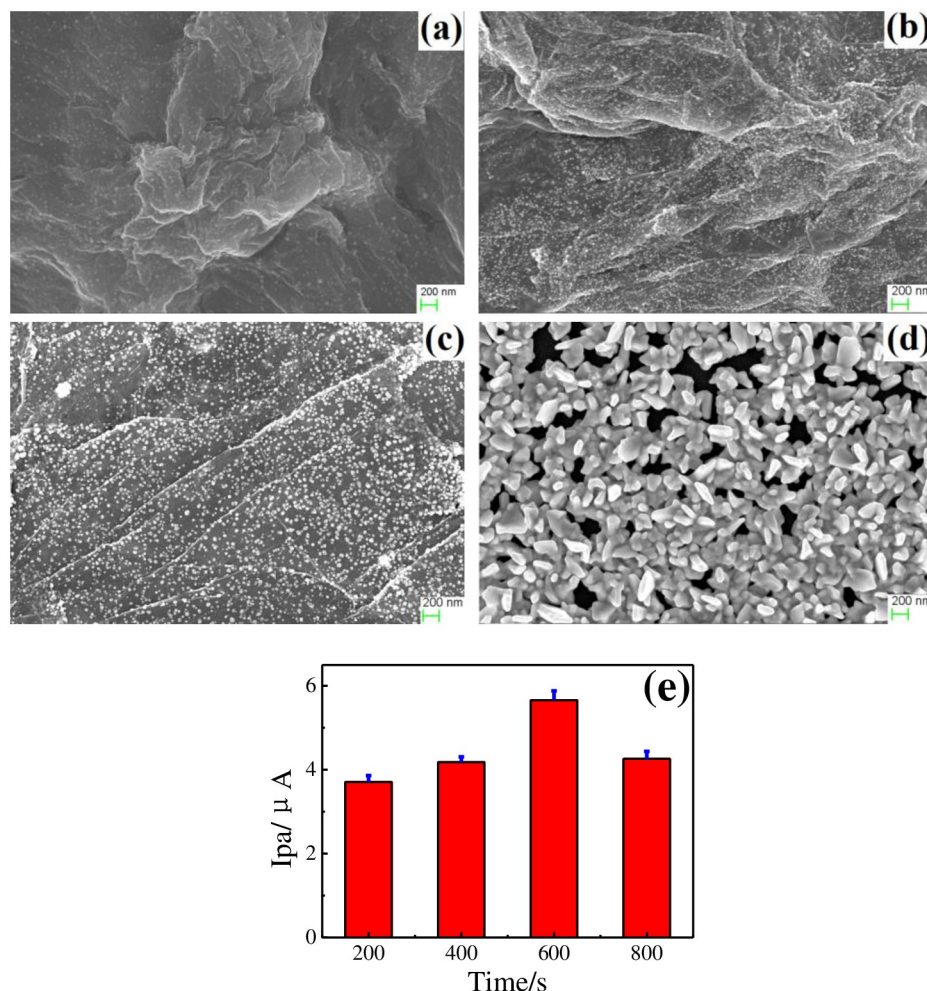
GCE│rGO-Au electrodes were prepared by casting 2.0 μL, 4.0 μL, 6.0 μL, 8.0 μL, and 10.0 μL of dispersion onto GCE, and electrochemical reduction in 0.1 M H_2SO_4 for 600 s. The Ipas of 20.0 μM DMY increased with the volume of dispersion modified onto GCE reached to 6.0 μL. More dispersion resulted in low peak currents. Hence, 6.0 μL of GO-HAuCl$_4$·3H$_2$O-nafion dispersion is fit for fabricating the GCE│rGO-Au electrode.

Time of electrochemical reduction. Different sizes of Au anchoring on rGO sheets with different electrochemical reduction time and their electrochemical performances toward 20.0 μM DMY are shown in Fig 7. With reduction time of 200 s, the smallest size of Au about 20 nm and a low coverage on GCE was observed (Fig 7a). The size of Au successively grew to 40 nm (Fig 7b), 60 nm (Fig 7c), and 100 nm (Fig 7d) as time raised up to 400 s, 600 s, and 800 s. The GCE│rGO-Au electrodes with different electrochemical reduction time displayed distinct performances toward 20.0 μM DMY (Fig 7e). The increases of reduction time from 200 s to 600 s resulted the increases of Ipas and the longer time of 800 s induced a worse sensing performance. As is known to all, higher coverage of Au and rGO modified onto electrode, larger available surface area and more active sites for DMY adsorbing and reacting can be

provided. The Au tended to form a compact surface as time increased up to 800 s, causing the lower current. Therefore, the reduction time of 600 s was selected.

Volume of polymerization mixture. The determination selectivity can be improved by the MIPs membrane as the target molecules of DMY can absorbed and enriched onto modified electrodes. However, the organic materials of MIPs are non-conductive. Five GCE│rGO-Au/MIPs electrodes were prepared via casting 1.0 μL, 3.0 μL, 5.0 μL, 7.0 μL, and 9.0 μL of polymerization mixture. The Ipas of 20.0 μM DMY were enhanced with the volumes of polymerization mixture cast onto GCE│rGO-Au electrode reached to 5.0 μL. More polymerization mixture resulted in decreased peak currents. Therefore, 5.0 μL of polymerization mixture is suitable to fabricate the GCE│rGO-Au/MIPs electrode.

Time of incubation and elution. The corresponding response currents of GCE│rGO-Au/MIPs electrode were recorded by DPV responses when it was immersed in PB containing 20.0 μM DMY with different time. The results indicated the Ipa reached the maximum value as the incubation time extended to 5 min, suggesting the fabricated sensor possesses a quick rebinding dynamics and the adsorption equilibrium can be achieved in short time.

Complete removal of templates from imprinted membrane after each run is important to obtain satisfactory selectivity results. Since H-bond is the major binding force between the templates and imprinted membrane, the acetic acid/ methanol mixture solution (1:1, v/v) was selected as eluent for removing DMY [25]. The results showed the Ipas of 20.0 μM DMY decreased gradually with increasing elution time till 30 min. The Ipa currents changed little with further increased elution time. Hence, 30 min was chosen as elution time.

pH value of PB. Fig 8 shows CV responses of GCE│rGO-Au/MIPs electrode in different pH values PB containing 20.0 μM DMY. The Ipa increased gradually when pH values changed from 5.0 to 6.0 and decreased at the higher pH values of 6.5 and 7.0. The largest Ipa was obtained at pH value of 6.0. It can be interpreted that the adsorption capacity of DMY on imprinted membrane was strongest and the activity of DMY was highest. As the pH values
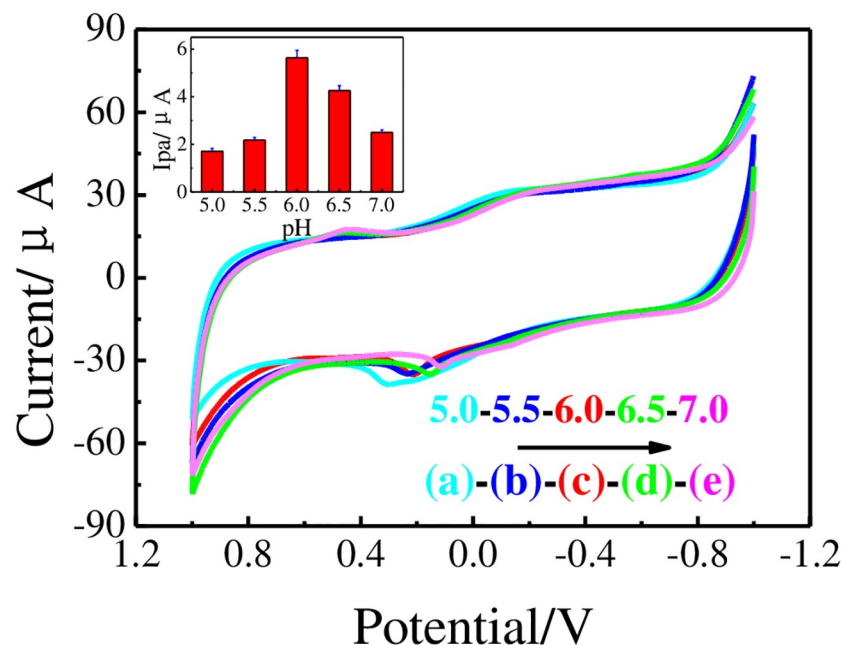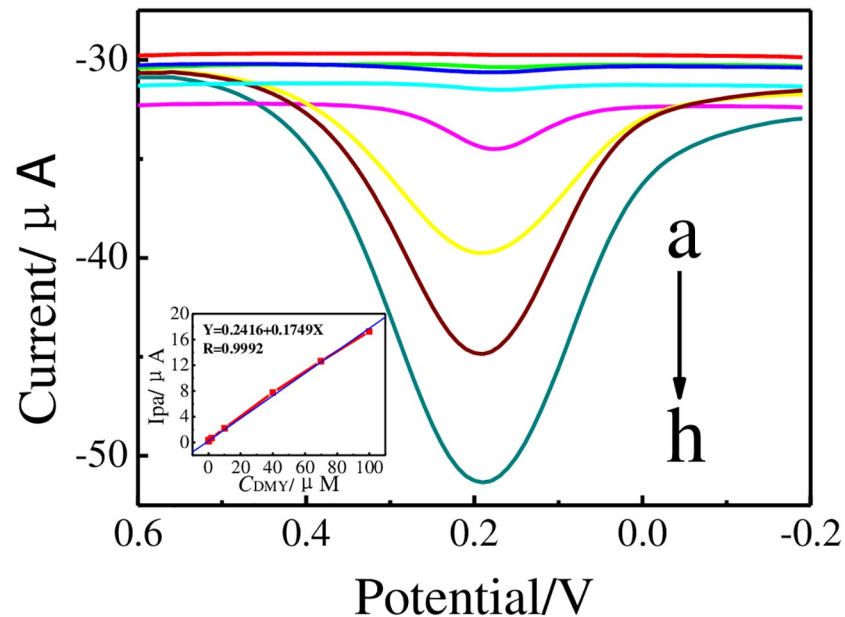

Fig 8. CVs of 20.0 μM DMY on GCE│rGO-Au/MIPs in PB varying pH levels 5.0 (a), 5.5 (b), 6.0 (c), 6.5 (d), and 7.0 (e). Insets: Ipa *vs*. pH.

Fig 9. DPVs of GCE│rGO-Au/MIPs in PB containing 0 (a), 0.02 (b), 0.2 (c), 2.0 (d), 10.0 (e), 40.0 (f), 70.0 (g), and 100.0 (h) μM of DMY. Insets: the calibration curve of C_{DMY} *vs*. Ipa.

https://doi.org/10.1371/journal.pone.0237583.g009

increased, the peak potentials shifted negatively, which indicated the protons participated during the electrochemical reaction [29–31]. Therefore, pH = 6.0 PB was selected as supporting electrolyte.

Detection of DMY

Under optimized experimental conditions, the DPV responses of GCE│rGO-Au/MIPs electrode recorded by different concentrations of DMY are demonstrated in Fig 9. The concentrations of DMY (C_{DMY}) in a wide linear detection range (LDR) of 2.0×10^{-8} to 1.0×10^{-4} M are proportional to well-defined Ipa currents. The linearization equation is: Ipa(μA) = $0.2416 + 0.1749 C_{DMY}$(μM) ($R = 0.9992$). A low limit of detection (LOD) obtained with the calculation is 1.2×10^{-8} M ($S/N = 3$).

Compared with some other DMY electrochemical sensors reported previously, the GCE│rGO-Au/MIPs electrode presented with the widest LDR and the lowest LOD (Table 1).

Table 1. Comparison of several typical DMY electrochemical sensors.

Electrode	Modifiers	LDR/M	LOD/M	Stability	Ref.
GCE	SWNTs[a]-nafion	$1.0 \times 10^{-7} – 1.0 \times 10^{-5}$	9.0×10^{-8}	7 days	[7]
GCE	DNA/En[b]/PGA[c]	$4.0 \times 10^{-8} – 2.0 \times 10^{-6}$	2.0×10^{-8}	7 days	[8]
GCE	Gr-nafion	$8.0 \times 10^{-8} – 2.0 \times 10^{-5}$	2.0×10^{-8}	56 days	[9]
GCE	rGO-Au/MIPs	$2.0 \times 10^{-8} – 1.0 \times 10^{-4}$	1.2×10^{-8}	56 days	This work

[a] SWNTs: Single walled carbon nanotubes.

[b] En: Ethylenediamine.

[c] PGA: Polyglutamic.

https://doi.org/10.1371/journal.pone.0237583.t001

Reproducibility, stability, and selectivity

The reproducibility of GCE│rGO-Au/MIPs electrode was valued with 10.0 μM DMY. A relative standard deviation (*RSD*) of 3.25% can be calculated after five successive assays using the same modified electrode. Five independent modified electrodes were used to study the electrode-to-electrode reproducibility. The obtained *RSD* was 2.88%. The reproducibility of modified electrode is acceptable.

The stability of GCE│rGO-Au/MIPs electrode is defined as the DPV response towards 10.0 μM DMY remained higher than 90.0% of its initial current. The DPV response towards 10.0 μM DMY preserved at 90.3% of its initial current after 8 weeks storage in dry and ambient condition, demonstrating long-term stability of modified electrode.

The substrates including coexisting interferents, structurally analogues, and inorganic ions that may affect current responses of GCE│rGO-Au/MIPs electrode towards a fixed DMY concentration of 10.0 μM were investigated. The selectivity is defined as a relative error of response lower than 5%. No interferences were arisen by addition of 20-fold concentrations of Cl^-, NO_3^-, K^+, Na^+, SO_4^{2-}, Fe^{2+}, Zn^{2+}, Mg^{2+}, Ca^{2+}, Mn^{2+}, and PO_4^{3-}, 10-fold concentrations of glucose, dopamine, uric acid, ascorbic acid, caffeine, glutamic acid, theophylline, rutin, quercetin, myricetin, and bisphenol A (Fig 10). The results indicate good selectivity of modified electrode (Table 2).

Real samples detection

The pretreatments of Ampelopsis grossedentata samples and quantification of DMY by HPLC were followed the literatures [7, 8]. Briefly, a certain amount of sample was mixed with water (liquid-solid ratio = 10:1), boiled for 60 min and filtered. The filtrate was collected and stored in refrigerator. The precipitates were dispersed in ethanol and analyzed as real samples. The quantification of DMY by HPLC was performed on a 4.6×150 mm C18 column combined with an ultraviolet-vis detector (290 nm). The mobile phase with a flow rate at 1.0 mL·min^{-1} is

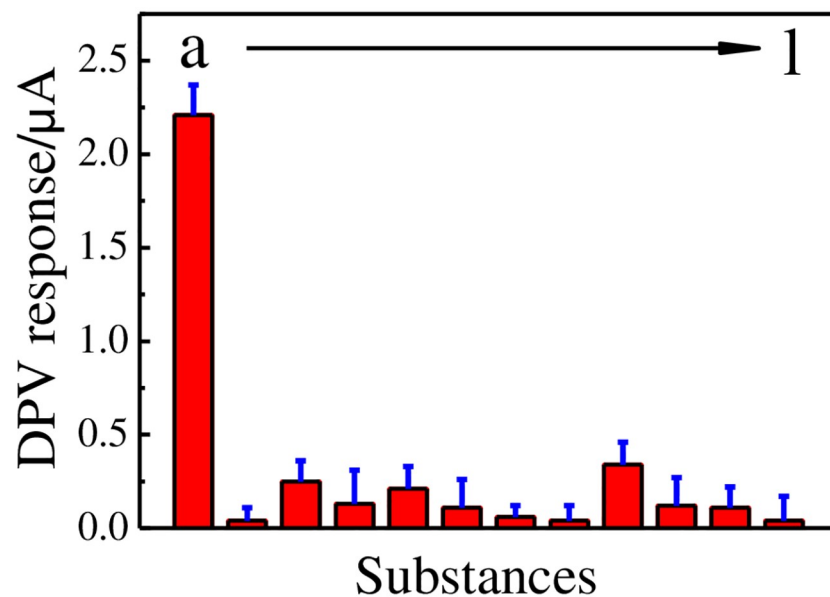**Fig 10. DPV responses of 10.0 μM of DMY (a), 0.1 mM of glucose (b), dopamine (c), uric acid (d), ascorbic acid (e), caffeine (f), glutamic acid (g), theophylline (h), rutin (i), quercetin (j), myricetin (k), and bisphenol A (l) on GCE│rGO-Au/MIPs.**

Table 2. The selectivity coefficients (k) values of some analogues on GCE│rGO-Au/MIPs.

Substances	DPV responses/μA	k
DMY	2.21	-
Glucose	0.04	55.25
Dopamine	0.25	8.84
Uric acid	0.13	17.00
Ascorbic acid	0.21	10.52
Caffeine	0.11	20.09
Glutamic acid	0.06	36.83
Theophylline	0.04	55.25
Rutin	0.34	6.50
Quercetin	0.12	18.41
Myricetin	0.11	20.09
Bisphenol A	0.04	55.25

https://doi.org/10.1371/journal.pone.0237583.t002

Table 3. Determination results of DMY in Ampelopsis grossedentata by DPV and HPLC.

	DPV (n = 3)					HPLC (n = 3)	
Sample	Amount found (mg·L^{-1})	RSD (%)	Added (mg·L^{-1})	Total found (mg·L^{-1})	Recovery (%)	Amount found (mg·L^{-1})	RSD (%)
1#	2.78	2.53	2.00	4.70	96.0	2.75	3.12
2#	2.73	4.02	2.00	4.66	96.5	2.75	3.52
3#	2.64	3.44	2.00	4.72	104.0	2.74	2.65

https://doi.org/10.1371/journal.pone.0237583.t003

0.1% phosphate/methanol solution (v/v = 70:30). The contents of DMY in real samples by calculating from the linear regression equation with standard solution are displayed in Table 3. Furthermore, the results obtained by HPLC and standard addition methods displayed no significant statistically difference, confirming the reliability of proposed method.

Conclusions

In summary, the sensitive, selective, and reliable electrochemical sensing platform based on double-layered membranes modified GCE for DMY determination was fabricated. The electrochemical reduction and polymerization strategies involved in the electrode modifying procedures combined the advantages of in-situ, controllable, facile, rapid, high usage, and environmental friendly. The fabricated modified electrode also showed superiorities of long-term stability, wide LDR, and low LOD compared with several other DMY electrochemical sensors due to the synergistic effects originated from composites. The practical applications of electrochemical sensor were confirmed by measuring real samples. The methodologies in preparation of MIPs-based composites and fabrication of sensing platform are universal, which possess widespread applications in the field of Chinese traditional herbal medicines analysis and quality monitoring.

Author Contributions

Conceptualization: Hongwei Lin, Xin Yang.

Formal analysis: Hongwei Lin.

Investigation: Jing Hu, Renjie Zhou, Hongwei Lin.

Project administration: Xin Yang.

Resources: Hongwei Lin.

Supervision: Feilong Hu, Xin Yang.

Validation: Qiuyuan Wei.

Writing – original draft: Qiuyuan Wei.

Writing – review & editing: Feilong Hu.

References

1. Liu D, Mao Y.Q., Ding L.J., Zeng X.A., Dihydromyricetin: A review on identification and quantification methods, biological activities, chemical stability, metabolism and approaches to enhance its bioavailability. *Trends Food Sci. Technol.* 2019, 91:586–597. https://doi.org/10.1016/j.tifs.2019.07.038 PMID: 32288229

2. Ye L.Y., Wang H.J., Duncan S.E., Eigel W.N., O'Keefe S.F., Antioxidant activities of Vine Tea (Ampelopsis grossedentata) extract and its major component dihydromyricetin in soybean oil and cooked ground beef. *Food Chem.* 2015, 172:416–422. https://doi.org/10.1016/j.foodchem.2014.09.090 PMID: 25442572

3. Jin M.Y., Ding Y., Zhang T., Cai Z.Z., Tao J.S., Simultaneous determination of dihydromyricetin and resveratrol in Ampelopsis sinica (Miq.) W.T. Wang by high- performance liquid chromatography coupled with a diode array detection method. *J. Chromatogr. Sci.* 2014, 52:339–343. https://doi.org/10.1093/chromsci/bmt036 PMID: 23616429

4. Du Q.Z., Cai W.J., Xia M., Ito Y., Purification of (+)-dihydromyricetin from leaves extract of Ampelopsis grossedentata using high-speed countercurrent chromatograph with scale-up triple columns. *J. Chromatogr. A* 2002, 973:217–220. https://doi.org/10.1016/s0021-9673(02)01092-0 PMID: 12437181

5. Tong Q., Hou X.L., Fang J.G., Wang W.Q., Xiong W., Liu X., et al. Determination of dihydromyricetin in rat plasma by LC-MS/MS and its application to a pharmacokinetic study. *J. Pharm. Biomed. Anal.* 2015, 114:455–461. https://doi.org/10.1016/j.jpba.2015.06.030 PMID: 26133104

6. Nan G.J., Sun J., Ding M.W., Yang X., Yang G.D., Interaction behavior between myricetin and dihydromyricetin with pepsin by spectroscopic and docking methods. *J. Mol. Liq.* 2016, 223:128–135.

7. Xu Y., Wang F., Wang L., Zhao F.Y., Yang B.C., Ye B.X., Sensitive voltammetric sensor of dihydromyricetin based on Nafion/SWNT-modified glassy carbon electrode. *J. Solid State Electrochem.* 2012, 16:1473–1480.

8. Zou L.N., Xu Y., Luo P.L., Zhang S.S., Ye B.X., Electrochemical detection of dihydromyricetin using a DNA immobilized ethylenediamine/polyglutamic modified electrode. *Analyst* 2012, 137:414–419. https://doi.org/10.1039/c1an15720e PMID: 22108641

9. Wang F., Yu X., Li H.J., Li M., Feng Q.M., Graphene-nafion composite film modified electrode for voltammetric sensor for determination of dihydromyricetin. *J. Chin. Chem. Soc.* 2013, 60:1019–1026.

10. Yang X., Ouyang Y.J., Wu F., Hu Y.J., Ji Y., Wu Z.Y., Size controllable preparation of gold nanoparticles loading on graphene sheets@cerium oxide nanocomposites modified gold electrode for nonenzymatic hydrogen peroxide detection. *Sens. Actuators B* 2017, 238:40–47.

11. Yao Z.F., Yang X., Niu Y.Y., Wu F., Hu Y.J., Yang Y.Q., Voltammetric dopamine sensor based on a gold electrode modified with reduced graphene oxide and manganic manganous oxide on gold nanoparticles. Microchim. *Acta* 2017, 184:2081–2088.

12. Govindhan M., Amiri M., Chen A.C., Au nanoparticle/graphene nanocomposite as a platform for the sensitive detection of NADH in human urine. *Biosens. Bioelectron.* 2015, 66:474–480. https://doi.org/10.1016/j.bios.2014.12.012 PMID: 25499660

13. Piovesan J.V., Santana E.R., Spinelli A., Reduced graphene oxide/gold nanoparticles nanocomposite-modified glassy carbon electrode for determination of endocrine disruptor methylparaben. *J. Electroanal. Chem.* 2018, 813:163–170.

14. Althagafi I.I., Ahmed S.A., El-Said W.A., Fabrication of gold/graphene nanostructures modified ITO electrode as highly sensitive electrochemical detection of Aflatoxin B1. *PLoS ONE* 2019, 14:e0210652. https://doi.org/10.1371/journal.pone.0210652 PMID: 30650140

15. Kıran T.R., Yola M.L., Atar N., Electrochemical sensor based on Au@nitrogen-doped carbon quantum dots@Ag core-shell composite including molecular imprinted polymer for metobromuron recognition. *J. Electrochem. Soc.* 2019, 166:H691–H697.

16. Özkana A., Atar N., Yola M.L., Enhanced surface plasmon resonance (SPR) signals based on immobilization of core-shell nanoparticles incorporated boron nitride nanosheets: Development of molecularly imprinted SPR nanosensor for anticancer drug, etoposide. *Biosens. Bioelectron.* 2019, 130:293–298. https://doi.org/10.1016/j.bios.2019.01.053 PMID: 30776616

17. Kıran T.R., Atar N., Yola M.L., A methyl parathion recognition method based on carbon nitride incorporated hexagonal boron nitride nanosheets composite including molecularly imprinted polymer. *J. Electrochem. Soc.* 2019, 166:H495–H501.

18. Yao Z.F., Yang X., Liu X.B., Yang Y.Q., Hu Y.J., Zhao Z.J., Electrochemical quercetin sensor based on a nanocomposite consisting of magnetized reduced graphene oxide, silver nanoparticles and a molecularly imprinted polymer on a screen-printed electrode. *Microchim. Acta* 2018, 185:70–78.

19. Özcan N., Medetalibeyoglu H., Akyıldırım O., Atar N., Yola M.L., Electrochemical detection of amyloid-β protein by delaminated titanium carbide MXene/multi-walled carbon nanotubes composite with molecularly imprinted polymer. *Mater Today Commun.* 2020, 23:101097.

20. Kadirsoy S., Atar N., Yola M.L., Molecularly imprinted QCM sensor based on delaminated MXene for chlorpyrifos detection and QCM sensor validation. *New J. Chem.* 2020, 44:6524–6532.

21. Zhou T., Tao Y., Jin H., Song B., Jing T., Luo D., et al. Fabrication of a selective and sensitive sensor based on molecularly imprinted polymer/acetylene black for the determination of azithromycin in pharmaceuticals and biological samples. *PLoS ONE* 2016, 11:e0147002. https://doi.org/10.1371/journal.pone.0147002 PMID: 26820753

22. Govindhan M., Chen A.C., Simultaneous synthesis of gold nanoparticle/graphene nanocomposite for enhanced oxygen reduction reaction. *J. Power Sources* 2015, 274:928–936.

23. Yang X., Wu F., Chen D.Z., Lin H.W., An electrochemical immunosensor for rapid determination of clenbuterol by using magnetic nanocomposites to modify screen printed carbon electrode based on competitive immunoassay mode. *Sens. Actuators B* 2014, 192: 529–535.

24. Yang X., Ouyang Y.J., Wu F., Hu Y.J., Zhang H.F., Wu Z.Y., In situ&controlled preparation of platinum nanoparticles dopping into graphene sheets@cerium oxide nanocomposites sensitized screen printed electrode for nonenzymatic electrochemical sensing of hydrogen peroxide. *J. Electroanal. Chem.* 2016, 777:85–91.

25. Bai H.P., Wang C.Q., Chen J., Pen J., Cao Q.E., A novel sensitive electrochemical sensor based on in-situ polymerized molecularly imprinted membranes at graphene modified electrode for artemisinin determination. *Biosens. Bioelectron.* 2015, 64:352–358. https://doi.org/10.1016/j.bios.2014.09.034 PMID: 25259878

26. Yang X., Wu F., Ouyang Y.J., Hu Y.J., Zhang H.F., Ji Y., Zinc oxide nanoparticles decorated on graphene sheets@cerium oxide nanocomposites to sensitize gold electrode for the nonenzymatic hydrogen peroxide detection. *J. Electrochem. Soc.* 2016, 163:834–839.

27. Cui D.D., Su L., Li H.J., Li M.J., Li C.P., Xu S., et al. Non-enzymatic glucose sensor based on micro-/nanostructured Cu/Ni deposited on graphene sheets. *J. Electroanal. Chem.* 2019, 838:154–162.

28. Hossain M.F., Park J.Y., Fabrication of sensitive enzymatic biosensor based on multi-layered reduced graphene oxide added PtAu nanoparticles-modified hybrid electrode. PLoSONE 2017, 12:e0173553.

29. Yang X., Zhang F., Hu Y.J., Chen D.Z., He Z.Q., Xiong L.Z., Gold nanoparticals doping graphene sheets nanocomposites sensitized screen-printed carbon electrode as a disposable platform for voltammetric determination of guaiacol in bamboo juice. *Int. J. Electrochem. Sci.* 2014, 9:5061–5072.

30. Yang S.R., Yang X., Tang R., Xiong L.Z., Yang Y.Q., Hu Y.J., et al. A novel rutin electrochemical sensor using reduced graphene oxide/magnetite/silver nanoparticle- molecularly imprinted polymer composite modified electrode. *Int. J. Electrochem. Sci.* 2018, 13:2483–2497.

31. Yola M.L., Necip Atar N., Development of molecular imprinted sensor including graphitic carbon nitride/N-doped carbon dots composite for novel recognition of epinephrine. *Composites Part B* 2019, 175:107113.